Datum
2024-01-23

Dnr
2018-004353

Projektnr
P2018-90048

Energimyndighetens titel på projektet – svenska Effektiva solenergiomvandlare baserade på halvledarnanoteknik
Energimyndighetens titel på projektet – engelska Efficient solar energy harvesting based on semiconductor nanotechnology

Universitet/högskola/företag Linköping University	Avdelning/institution IFM
Adress Campus Valla, 581 83 Linköping	
Namn på projektledare Galia Pozina	
Namn på ev övriga projektdeltagare Carl Hemmingsson	
Nyckelord: 5-7 st Wide bandgap semiconductors, epitaxial growth, III-nitrides, nanostructures, Purcell effect, nanoantenna, plasmonics.	

Förord

The project has been fully funded by the Swedish Energy Agency. We are very grateful to the Swedish Energy Agency for providing us with support to carry out this project, which we hope will further develop. We would like to thank everyone who has in some way contributed to the development of both technology and fundamental understanding of effects of light-matter interaction in semiconductors.

Innehållsförteckning

Box 310 • 631 04 Eskilstuna
Telefon 016-544 20 00 • Telefax 016-544 20 99
registrator@energimyndigheten.se
www.energimyndigheten.se
Org.nr 202100-5000

Sammanfattning

Den globala efterfrågan på förnybar energi, driven av de klimatförändringarna som vi ser av användningen av fossila energikällor, understryker behovet av effektiv energiomvandling. Breda bandgap halvledare som GaN, InGaN, AlGaN och galliumoxid spelar en avgörande roll i detta paradigmskifte och används inom energieffektiv belysning, högeffekts transistorer, omvandlare för solenergi och solenergibaserad vätgasproduktion. Målet med projektet var att utforska III-N-planara nanostrukturer med önskvärda egenskaper, såsom form, position och emissionsvåglängd, för att optimera hybridstrukturer. Dessa hybrider kombinerar halvledare och metallnanopartiklar och kan potentiellt användas för utveckling av fotoceller baserade på hybrid nanoantennkonceptet. Avancerade planara nanostrukturer baserade på III-nitrider utvecklades genom gas fas epitaxi. Studien visar att kristallografiska tillväxtriktningar spelar en avgörande roll för att bestämma den strukturella kvaliteten hos GaN nanostrukturer, vilket gör dem till utmärkta kandidater som optiska resonatorer och element för nanoantenner i avancerade elektroniska komponenter. Beroende på GaN nanostrukturernas orientering uppvisar de en förmåga att modifiera resonansfrekvensen i de optiska spektrumen hos hybridnanostrukturer som bildas av planara GaN nanotrådar och plasmoniska nanopartiklar. Möjligheten att kontrollera den kristallografiska tillväxtriktningen öppnar vägar för att förbättrad effektivitet i optoelektroniska komponenter och lovar ytterligare framsteg inom ljusabsorption och emission, vilket är avgörande för effektiv solenergiinsamling och omvandling. I projektet utforskade vi olika teoretiska metoder för att förklara de modifierade optiska egenskaperna, ökad emission och förekomsten av nya luminescenslinjer i resonatorer med olika design. Vi har i studien påvisat en potential för stark interaktion mellan excitoner och kavitetsmoder i meso-kaviteter av olika former. Dessutom har vi utvecklat en process för plasmaassisterad halid gas fas epitaxi för att odla InGaN halvledare vid lägre temperaturer. Tack vare plasmat effektiviseras aktiveringen av ammoniak-prekursorn vid lägre temperaturer vilket medför en högre tillväxthastighet. Trots utmaningar med strukturell kvalitet och relativt låg inkorporering av indium är konceptet att använda plasma för ammoniakaktivering mycket lovande. Fortsatt teknologisk utveckling kan leda till III-N strukturer med funktioner i det hela synliga spektrala området. Utmaningar kvarstår, särskilt när det gäller utformningen av effektiva likriktande dioder för optiska frekvenser. Kontinuerlig forskning är avgörande för att övervinna dessa utmaningar och bidra till utvecklingen av energieffektiva teknologier och hållbara energisystem.

Summary

The global demand for renewable energy, driven by environmental concerns, highlights the necessity for efficient power conversion. Wide bandgap semiconductors such as GaN, InGaN, AlGaN, and gallium oxide play pivotal roles in this paradigm shift, finding applications in energy-efficient lighting, high-power transistors, solar light converters, and solar-driven water splitting for clean hydrogen fuel production. The goal of the project was the exploration of III-N

planar nanostructures with desirable properties such as shape, position, and emission wavelength that can be used for optimization of hybrid structures. These hybrids combine semiconductor counterpart and metal nanoparticles, with potential for developing a prototype photocell based on the hybrid nanoantenna concept. Advanced planar nanostructures based on III-nitrides were developed and explored through epitaxial deposition techniques within the project. The study reveals that the crystallographic growth directions play a pivotal role in determining the structural quality of GaN nanostructures, making them prime candidates for optical resonators and building blocks for nano-antennas in advanced electronic devices. We have found that GaN nanostructures, depending on their orientation on the substrate, show different ability to modify resonance frequency in the optical spectra of hybrid nanostructures formed by the combination of semiconductor nanowires and plasmonic silver nanoparticles. The ability to control the crystallographic growth direction opens avenues for enhanced efficiency in optoelectronic devices, promising advancements in light absorption and emission crucial for solar energy harvesting and conversion. The study explored different theoretical approaches to explain modified optical properties, emission enhancement, and the appearance of new luminescence lines in resonators with different designs. The study demonstrates the potential for strong interaction between excitons and cavity modes in meso-cavities of various shapes. Also, plasmonic-polaritonic phenomena in layered structures have been investigated, offering design principles to reduce losses and enhance spontaneous emission probabilities in visible and infrared energy regions. Moreover, we developed a plasma-assisted halide phase vapor epitaxy process for growing InGaN layers at lower temperatures. We have utilized a plasma source to enhance the efficiency of ammonia decomposition at low temperatures and, thereby, increased the growth rate. Despite challenges with structural quality and relatively low incorporation of indium, the concept of using plasma for ammonia activation is very promising. Continued technological development could lead to the InGaN structures with the operation range covering the entire visible spectral range. Challenges persist, especially in designing rectifying diodes for effective operation at optical frequencies. Continuous investigation is crucial to overcome these challenges and contribute to the development of energy-efficient technologies and sustainable energy systems.

Inledning/Bakgrund

The development of renewable sources of energy is a strategic priority globally, with a focus on improving the efficiency of power conversion. The increasing global demand for energy should be considered in frame of the environmental impact of fossil fuel combustion, which increases the importance of searching for possible clean and sustainable alternative of energy sources, such as wind and wave energy, solar energy, or hydrogen energy to name some of them.

Recently, there has been a significant development of wide bandgap semiconductors such as GaN and its alloys with In and Al, or gallium oxide (Ga_2O_3)

that could be alloyed with Zn. Today, these wide bandgap materials are frequently used for various applications, especially for energy-efficient light sources, which are already on the market (white LEDs). Other applications for high power high-frequency transistors are demonstrated in an operational environment, showcasing its functionality and potential. For III-nitrides in photovoltaic devices specifically, their technology readiness level (TRL) is lower than their use in other electronic devices, though there has been research and development exploring the utilization of III-nitrides for solar cells in a laboratory environment with advancements in increasing conversion efficiency. The III-nitrides has clear advantages over traditional silicon-based solar cells. The tunable bandgap of III-nitrides, along with their reliability, thermal and chemical stability, and capability to absorb the entire solar spectrum, makes them a promising solution for addressing challenges associated with defects and polarization charges. Nanotechnology, specifically focusing on III-nitride nanostructures, is an approach that can address challenges and improve efficiency of photovoltaic devices. These properties, coupled with the ability to produce various III-N nanostructures like planar nanodisk and nanowire structures, offer a pathway to achieve high conversion efficiency and improved performance in photovoltaic (PV) devices. This is particularly significant for applications in space environments, such as spacecraft and satellites, where conventional power sources may be impractical or insufficient.

Applications of III-nitrides can be further explored for electrolysis of water via the generation of the electricity by the photovoltaic cells, which is then used to power the water splitting into hydrogen and oxygen. The use of solar-driven water splitting has gained attention as a means of producing clean and sustainable hydrogen fuel. Hydrogen is considered a versatile energy carrier and can be used in fuel cells to generate electricity or as a feedstock for various industrial processes.

The concept of next-generation solar energy converters based on optical rectennas comprises an optical nanoantenna for efficient solar light absorption and a high-frequency tunneling diode that rectifies the alternating current field across the antenna, providing direct current power. In theory, rectennas could harvest energy from heat. However, the problem is that in order to capture radiation, rectennas have to be extraordinarily tiny, but the smaller they are, the more their resistance grows, which reduces their power output. Another challenge is related to high-frequency diodes in optical rectennas, specifically in achieving a balance between low resistance and high responsivity [1]. Metal–insulator–metal (MIM) diodes face difficulties in simultaneously achieving low resistance and high responsivity, essential for efficient rectification, and are still a bottleneck prohibiting the development of optical rectenna.

The project was focused on exploring and expanding wide bandgap semiconductor materials for use as optical nanoantennas in UV range. For the production of III-nitrides and III-oxides we use epitaxial deposition techniques such as halide vapor phase epitaxy (HVPE) and metal-organic vapor phase epitaxy (MOVPE).

Genomförande

The research methodology focuses on leveraging the expertise in growth optimization and optical spectroscopy of wide bandgap semiconductors to develop controlled fabrication methods and fundamental understanding of properties of nanoantenna structures.

Modelling

To optimize the growth parameters such as precursor ratio, we have used the transport model based on numerical solution of the nonlinear coupled partial differential equations for the conservation of mass (i.e. continuity equation), energy, momentum (i.e. Navier–Stokes equation), and individual species. For calculations, we have used COMSOL Multiphysics software with CAD Import Module, CFD Module and Chemical Reaction Engineering Module.
The following equations have been used to describe the system. The energy equation is written as:

$$\nabla \cdot \mathbf{j}_i + \rho(\mathbf{u} \cdot \nabla)\omega_i = R_i \quad , \qquad (1)$$

where ρ is a density of gas, $\mathbf{u}$ - is velocity and ω and R are cylindrical coordinates, respectively.
Species continuity equation is written as:

$$\mathbf{N}_i = \mathbf{j}_i + \rho\mathbf{u}\omega_i \quad , \qquad (2)$$

where

$$\mathbf{j}_i = -\left(\rho\omega_i \textstyle\sum_k D_{ik}\,\mathbf{d}_k + D_i^T \frac{\nabla T}{T}\right). \qquad (3)$$

We denote:

$$\mathbf{d}_k = \nabla\chi_k + \frac{1}{p_A}\left[(\chi_k - \omega_k)\nabla p_A + \frac{\rho\omega_k z_k}{M_k} F\nabla V - \textstyle\sum_l \frac{\rho\omega_l z_l}{M_l} F\nabla V\right], \qquad (4)$$

and

$$\chi_k = \frac{\omega_k}{M_k} M_n \ , \quad M_n = \left(\textstyle\sum_i \frac{\omega_i}{M_i}\right)^{-1} \qquad (5)$$

Navier-Stokes (momentum) equation reads as:

$$\rho(\mathbf{u} \cdot \nabla)\mathbf{u} = \nabla \cdot \left[-\rho\mathbf{I} + \mu(\nabla\mathbf{u} + (\nabla\mathbf{u})^T) - \frac{2}{3}\mu(\nabla \cdot \mathbf{u})\mathbf{I}\right] + \mathbf{F}\,, \qquad (6)$$

and the mass equation as:

$$\nabla \cdot (\rho\mathbf{u}) = 0 \qquad (7)$$

The flow velocities have been obtained from the energy equation (1) and momentum equation (6), while the gas concentration profiles are obtained from the conservation of mass, equation (7) and individual species (2). In the calculations, the flow was assumed to be incompressible.
The cavity mode energies, their Q-factors, and the spatial distribution of the cavity modes intensity have been calculated by solving the Maxwell equations using the COMSOL Multiphysics software.

Growth

The growth of GaN was done using halide vapor phase epitaxy (HVPE) and metal-organic vapor phase epitaxy (MOVPE), with ammonia as the nitrogen source. Alternatively, to expand the operation region to deep UV spectral range, the growth of Ga_2O_3 structures and films has been also studied using HVPE process at temperatures 850-1000 °C. For producing alloys such as InGaN for operation in visible and red spectral region, the growth temperature should be reduced to 600 °C, i.e. much lower compared to the growth of GaN, which is synthesized at 1000 °C. The challenge is to reduce the growth temperature of III-nitrides in HVPE or MOVPE processes to ~500-600 °C, i.e. to temperatures necessary to prevent thermal segregation of InGaN. The reason is that the cracking efficiency of ammonia, which is the only possible precursor of nitrogen in the vapor phase epitaxial deposition, sharply reduces at temperatures below 1000 °C, which results in low growth rates and bad crystal quality [2].

The idea was to increase the possibility of ammonia activation at low temperature using plasma source as schematically shown in Fig.1a that was introduce in the HVPE reactor (Fig.1b).

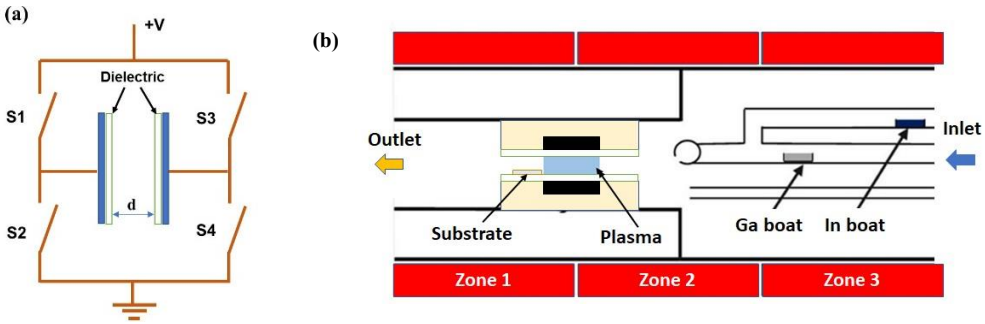

Figure 1. (a) Schematic drawing of plasma generation dielectric barrier discharge. High-voltage bridge to switch polarity between electrodes with the electrode distance d. (b) Schematic drawing of the HVPE reactor.

The synthesis process of GaN nanostructures was based on the selective area MOVPE. The pattern was etched using focused ion beam (FIB) in Si_3N_4 mask film deposited on the top of GaN layer. In FIB, the following parameters were used: the Ga ion beam energy of 30 keV and the probe current of 450 pA (see Fig 2). After etching, MOVPEcvd growth has been applied at temperature of ~1000 °C to fabricate GaN planar nanostructures.

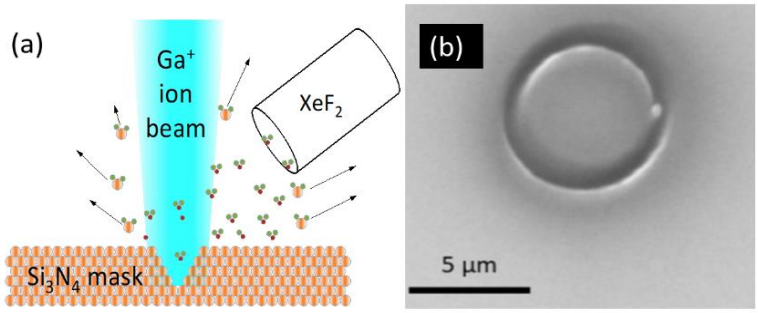

Figure 2. (a) Schematic drawing of the FIB etching of mask layer using Ga ions and a xenon difluoride gas for controlling parasitic growth. (b). Example of the etched pattern in the form of the ring.

Optical spectroscopy

For characterization, we employ a LEO 1550 Gemini SEM combined with MonoCL4 system having a liquid-He-cooled stage for low-temperature cathodoluminescence (CL) measurements. Electron beam energy was kept to 5 keV for improved spatial acquisition limits of CL images and spectra (better than 100 nm). CL spectra and CL images have been acquired using a fast CCD detection system with liquid nitrogen cooling and a Peltier cooled UV-vis photomultiplier tube, respectively. The CL system is shown in Fig. 3a. Photoluminescence (PL) and time-resolved photoluminescence (TRPL) have been studied in the range from cryogenic to room temperatures with samples placed in a microstat providing temperatures in the range 5 – 300 K. The µ-TRPL setup allows high spatial resolution with the laser beam focused to a spot less than 1 µm in diameter. PL excitation was done by a triple harmonic (266 nm) from the Ti:sapphire femtosecond pulsed laser having frequency of 75 MHz. Signal acquisition was performed using Hamamatsu syncroscan streak camera with temporal resolution of ~20 ps. The PL setup is shown in Fig. 3b.

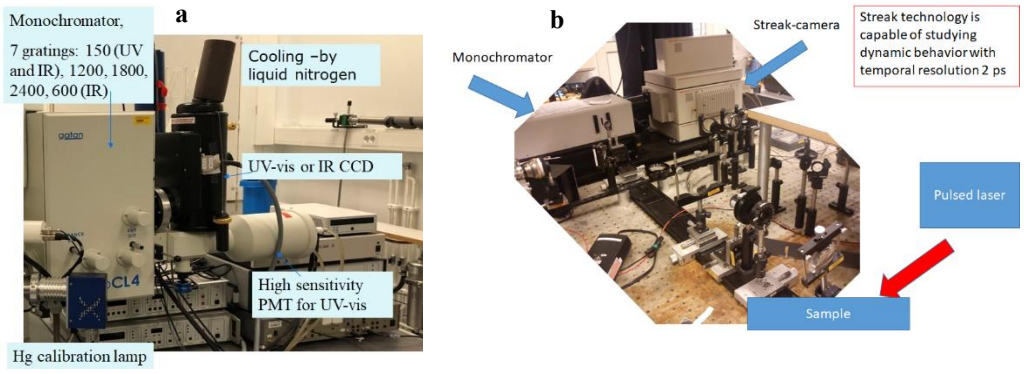

Figure 3. (a) CL system is coupled with SEM instrument. (b) Set-up for optical spectroscopy measurements.

Resultat

We have revealed a crucial effect of the crystallographic direction along which the growth is done on structural quality of nanowires. Two crystallographic orientations of planar GaN nanowires (NWs) along $[11\bar{2}0]$ and $[10\bar{1}0]$ directions were investigated. The coherent growth is confirmed for both directions as can be seen in Fig. 4a. However, the best morphology, crystalline and optical properties are found in the NWs fabricated along the $[10\bar{1}0]$ axis, which allows to utilize such structures as optical resonators and building blocks for nano-antennas. The geometrical shape and morphological properties are illustrated in Fig.4 b-e.

A high quality and resonator properties have been confirmed by the presence of Fabry-Perot modes in the CL spectra in the region of 1.8 eV- 2.5 eV for the NWs fabricated in the $[10\bar{1}0]$ direction, see Fig.5. The position and intensity of the Fabry-Perot peaks were explained by the small fluctuation of thickness of the structure and by the model based on the Purcell coefficient calculations, where the enhancement or reduction of the emission intensity for the Fabry-Perot peaks depend on the position of the emitter inside the planar NW.

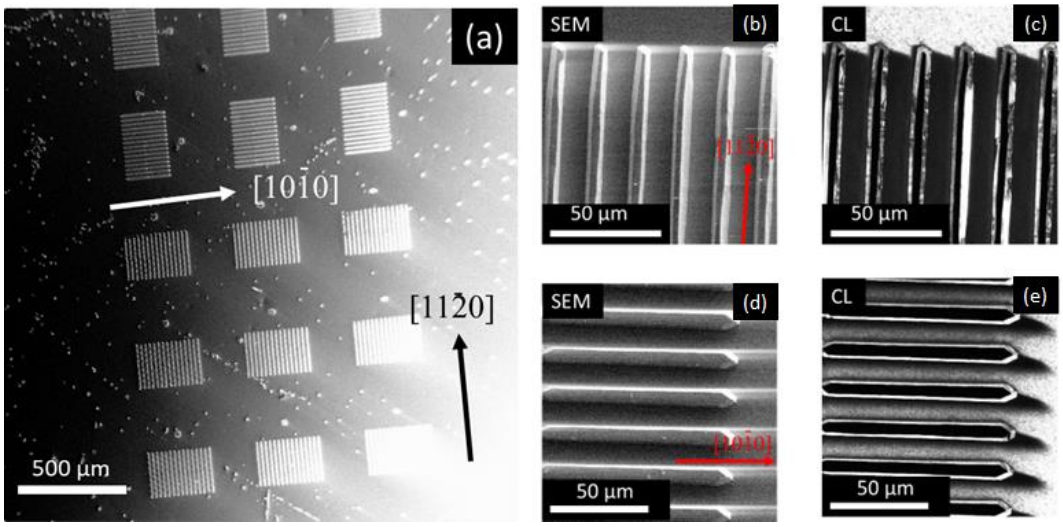

Figure 4. (a) An overview SEM image showing a pattern of planar GaN nanowires grown along two orthogonal crystallographic direction as indicated by arrows. (b,d) SEM images for the planar GaN NWs grown along $[11\bar{2}0]$ and $[10\bar{1}0]$ directions, respectively. (c, e) Panchromatic CL images measured simultaneously with SEM images for the same areas as in (b, d).

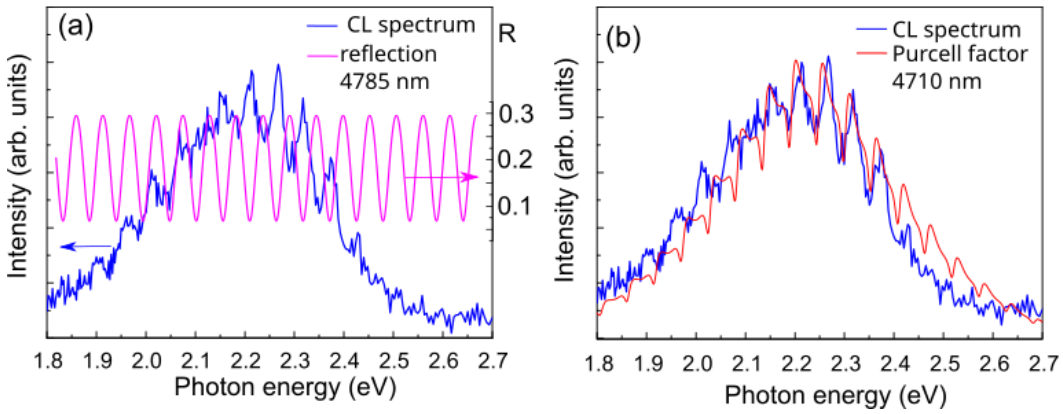

Figure 5. Experimental CL spectra together with reflection (a) and with the modal Purcell coefficient calculations (b). The Purcell factor was calculated for the emitter placed at 15 nm from the surface of the planar GaN NW. Thickness *d* of the structure used for calculations was slightly different (4785 and 4710 nm) demonstrating a strong dependence of the peak position on *d*.

For the layer of thickness d between two reflecting interfaces (i.e. cavity), the energies of Fabry-Perot modes can be calculated as:

$$E = \pi\hbar cM\ /(nd), \qquad (1)$$

where M is an integer, n is the refractive index of media, which gives the interval between the modes:

$$\Delta E = \pi\hbar c/(nd) \qquad (2)$$

For the CL band with energies between 2.0 eV and 2.5 eV, the integer M is between 33 and 42, which gives the positions of the Fabry-Perot modes in the aforesaid photon energy interval.

Other types of GaN planar nanostructures in the form of hexagons, which are analogue of micro-resonator supporting whispering gallery modes, demonstrated in the near band gap region a strong modification of the emission spectra compared to the emission of layer due to the interaction of the exciton with cavities modes. This case is illustrated in Fig.6 (a-d), where SEM images were taken simultaneously with CL maps at different temperatures. At 15 K, the CL image in Fig. 6d shows that the emission intensity is not uniformly distributed along the walls of the hexagon, which is also reflected in the emission spectra (Fig.6e,f). To investigate how the CL intensity is distributed within the hexagon, we have measured CL images at energies from 3.47 eV to 3.02 eV. Figure 7 shows examples of CL maps obtained at different detection energies. The CL image taken at 3.47 eV (Fig. 7a) shows that the emission comes from the GaN layer, and not from the hexagon. However, when we change the detection energy to 3.44 eV (Fig. 7b), we can see a rather uniform distribution of CL intensity along the outer walls. The emission pattern along the hexagon's walls has become more spot-like at detection energies within the band peaking at ~3.3 eV (example in Fig. 7c). Even at lower energy, below a peak at 3.3 eV we could detect the CL signal concentrated mainly in the corners of the internal hexagon.

A numerical analysis of exciton-polariton modes has shown that some strongly localized cavity modes can have high Purcell coefficients and can strongly interact

with the GaN exciton. We model the structures of GaN microcavities using the simplified case of a two-dimensional (2D) hexagon, as shown in Figure 8a.

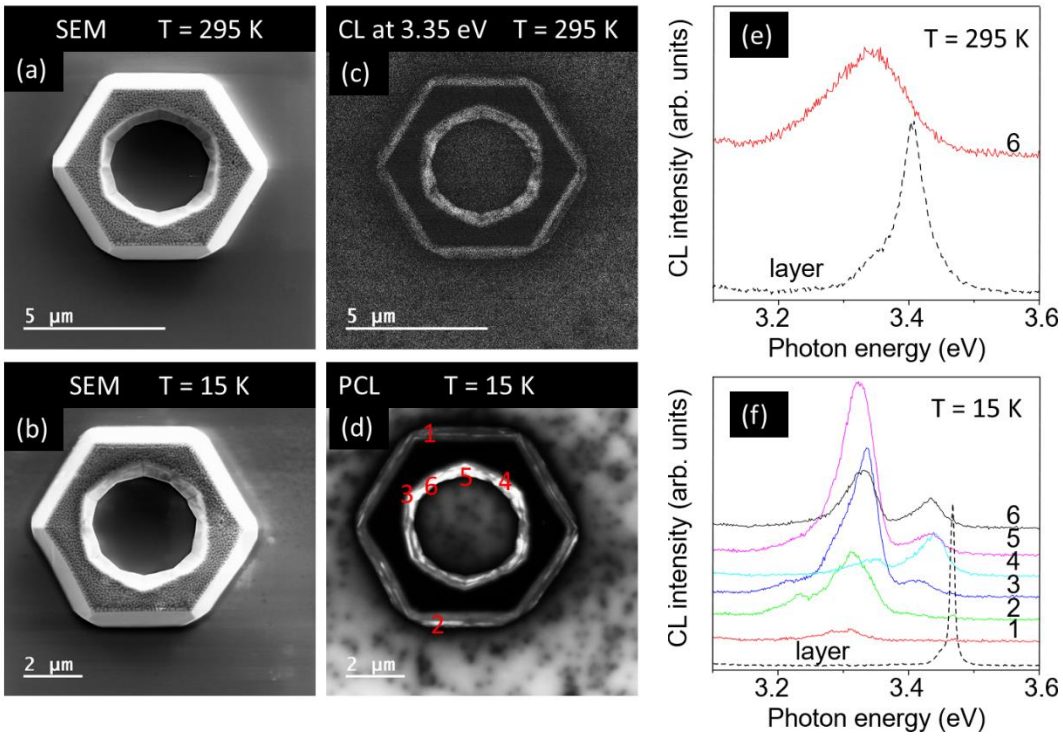

Figure 6. (a), (b) – SEM images of the hexagon cavity measured at room temperature and at 15 K simultaneously with the CL images shown in (c),(d), respectively. (e) An example of the CL spectrum taken in point 6 of the image in (d) measured at 295 K is compared with the emission from the GaN layer (dashed line). (f) CL spectra measured at 15 K at several points, as indicated in image (d). The reference spectrum from the GaN layer measured at 15 K is also shown (dashed line).

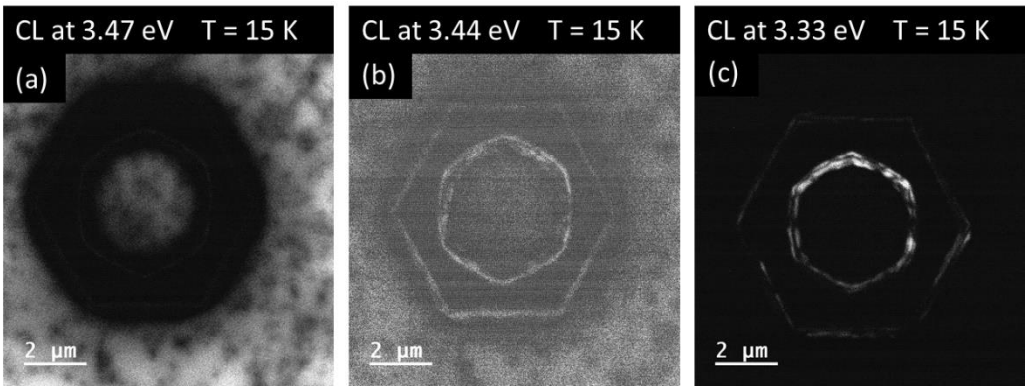

Figure 7. Monochromatic CL images taken for the same hexagon as in Figure 3 at a temperature of 15 K at different detection energies: (a) 3.47 eV, (b) 3.44 eV, (c) 3.33 eV.

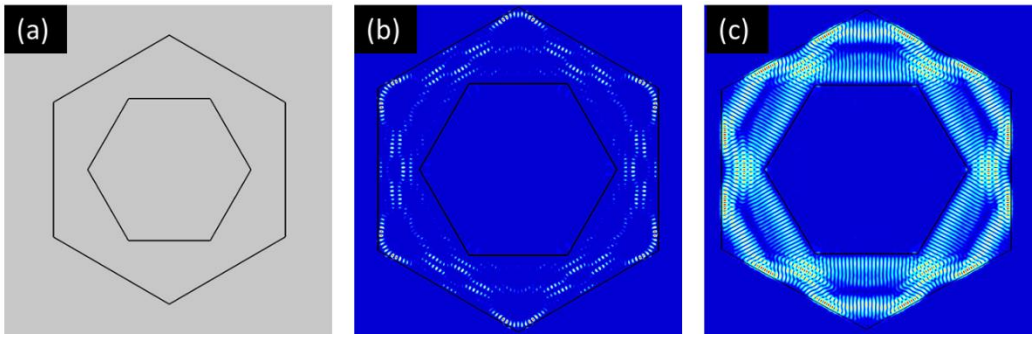

Figure 8. (a) Schematic drawing of a 2D hexagonal structure used for numerical simulation. The sizes for the radii are as follows: 1.95 μm for the inner and 3.20 μm for the outer hexagon, respectively. (b),(c) Calculations of the distribution of electromagnetic field intensity for modes inside an ideal hexagonal resonator. Examples are shown for two modes with an energy of 3.26 eV (b) and 3.3 eV (c), respectively.

In the simulations, it was assumed that the microcavity material has no absorption; for refractive index of GaN we use n=2.6267. Calculations show that there are many different modes with an interval of 28 meV. The modes have different spatial distribution of electromagnetic wave intensity and different Q-factors. Fig. 8b and c show examples of the distribution of radiation intensity calculated for modes with an energy of 3.26 eV and 3.3 eV, respectively. It is clearly seen that modes have different localization and volume. Typically, the Q factor was rather low for most modes, except for a small number of resonator modes, where the Q factor was about 400 or higher.

The Purcell factor describing the ability of a resonator to increase the coupling of an ideal emitter with a vacuum field can be expressed as follows [3]:

$$\boldsymbol{F_p \approx \frac{3Q\lambda^3}{4\pi^2 n^3 V}}, \qquad (1)$$

where Q is the quality factor, λ is the cavity wavelength, n is the refractive index of the medium and V is the effective mode volume. For low Q factors (as in our case), still an enhancement of the local intensity of the emitter can occur for small volumes of cavity modes. A theoretical consideration of the interaction of the GaN exciton with cavity modes was done based on the Hamiltonian of the interaction between the exciton and the cavity modes. Such interaction can occur both in weak and in strong coupling regimes. The latter case can be accompanied by a pronounced splitting of the emission peaks as shown for modelled meso-cavities of different shapes, where it is demonstrated that Q-factors for the adjacent cavity modes as well as the strength of interaction with excitons can differ by few orders of magnitude. We calculated the cavity mode energies, their Q-factors, and spatial distribution of the cavity modes field by solving Maxwell's equations using numerical calculations for cavities with sizes to be equal to several wavelengths. The example of simulation is shown in Figures 9 for mesa-cavities of hexagonal shape.

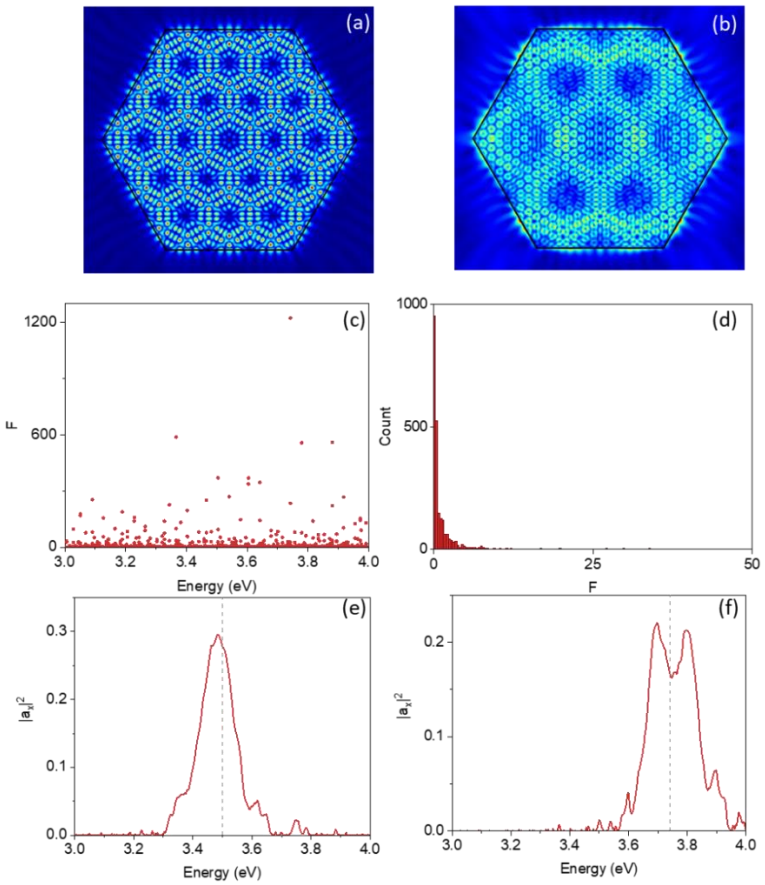

Figure 9. (a-b): The distribution of the electromagnetic field intensity of the modes inside the ideal hexagonal resonator with a side of 2 μm and refractive index of n = 3. (a) Example of a strong localized mode (3.2 eV, $Q = 5.2 \cdot 10^4$), (b) Example of a weakly localized mode (3.21 eV, $Q = 2.3 \cdot 10^3$). (c) Energy distribution of the Purcell coefficient (F), describing the strength of interaction of the cavity modes with an emitter, for the modes localized in the hexagon, (d) Histograms illustrating distribution of cavity modes depending on F. (e-f): Dependence of the excitonic contribution to the polaritonic state as a function of the energy of the polariton mode for hexagonal mesa-cavity. (e) Exciton energy ($w_0 = 3.5\ eV$) is located at the distance from the mode energy with a high F. (f) Exciton energy ($w_0 = 3.74\ eV$) is located nearby to the mode energy with a high F.

For studies of problems related to plasmonic-polaritonic phenomena, the Purcell effect in metal-dielectric layered structures (see Fig. 10a) was considered using theoretical approaches. We demonstrated how design of the structure can be used to control the properties of the metamaterial, the dispersion of a surface plasmon, and the value of the Purcell factor. We used silver as an example of metal and for dielectric, we used several materials. One of them was the organic light-emitting compound 4,4-Bis(N-carbazolyl)-1,1-biphenyl (CBP) that was previously studied for its suitability for silver-based plasmonic structures. The proposed metamaterial was consisting of alternating layers of metal and dielectric parallel to the xy plane (see Fig. 10a). The corresponding layer thicknesses are denoted by a and b, and the fraction of metal in the metamaterial is denoted as the filling factor:

$$\alpha = \frac{a}{a+b}$$

It was shown that a specific design of the layered structures can be chosen in a way to reduce the absorption of metal, i.e. reduce the losses, by shifting the peak of the local density of states toward lower energy (see Fig. 10b). In this case, the peak value of the Purcell coefficient was shifted to visible or infrared energy region, where the value of the Purcell coefficient is increased by one order of magnitude and, thus, a higher magnitude of the enhancement of the spontaneous emission probability can be reached.

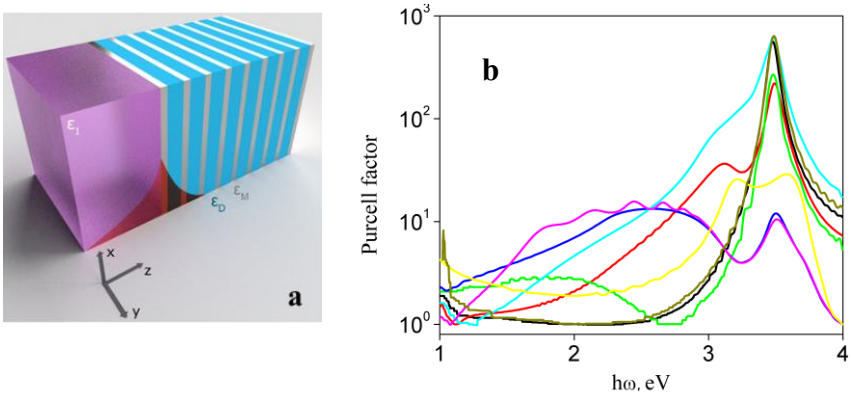

Figure 10. (a) Geometry and composition of the structure. Silver and blue colors denote metallic and dielectric (CBP) layers of metamaterial, respectively. The purple color denotes dielectric cladding layer (silica). The red color represents the electric field of the surface plasmon. (b) Dependence of the Purcell factor on frequency calculated for a silver/CBP metamaterial on silica substrate. Two values of α and different periods of the metamaterial are considered: 15 nm (black: α=0.8, red: α=0.2), 5 nm (green: α=0.8, blue: α=0.2) and 0.5 nm (cyan: α=0.8, and magenta: α=0.2). Surface plasmon propagating along the single interface for silver/CBP (yellow) and silver/silica (dark yellow).

III-nitrides planar nanocavities demonstrated a non-monotonic increase of some emission lines (i.e. its integral intensity) with increasing power of optical pumping. To explain the experimental results related to the enhancement of luminescence in planar nanostructures, we considered a general theoretical approach. It was shown that in meso-structures supporting several separated cavity modes (Fig.11a), the interaction of different modes with an exciton are comparable and the pattern of such strong interaction is rather complex, which leads to different fundamental effects, for example, a step-like increase of the exciton population, quantum beating and non-monotonic dependence of the ground polariton state in the system on the pumping. Fig. 11b illustrates the dependencies of the population of polariton levels in meso-cavity, supporting three cavity modes interacting with an exciton in the presence of exciton-exciton interaction. The behavior of the population of polariton modes on pumping (I) demonstrates a threshold behavior. When the pumping reaches a certain threshold value, the occupancy of the polariton modes increases sharply and then grows much faster. The magnitude of the hysteresis loop strongly depends on the magnitudes of the dissipations of the exciton and photon modes. With an increase in dissipation, the hysteresis loop decreases. It can be seen, that all four polaritonic modes (p1-p4) demonstrate hysteresis-like dependence, but for ground state polariton, there is non-monotonic behavior of the population on the

pumping. Such additional non-linear feature can be used to enhance the range of non-linear application of polaritons.

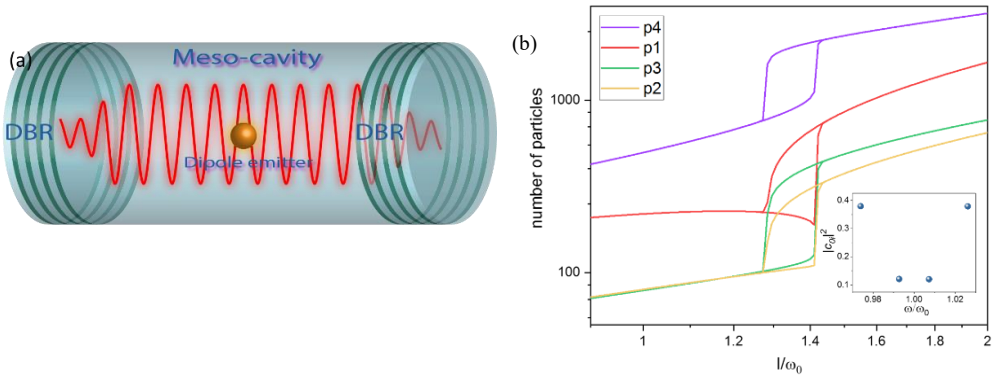

Figure 11. (a) Schematic representation of a meso-cavity with an emitter. The size of the cavity between two distributed Bragg reflectors (DBR) is about 10 radiation wavelengths in the material. (b) Dependence of the population of polariton modes on pumping. The low-energy mode (p1) has an anomalous bi-stability loop with non-monotonic dependence of occupancy on pumping. Inset: Hopfield coefficient illustrating excitonic contribution to polariton modes.

A study of the interaction of light and matter in strong and ultra-strong coupling regime at room temperature was done also in collaboration with several international research groups. The system was so called Tamm plasmon cavities, where silver was deposited on specifically designed periodic structure of SiO_2 and Ta_2O_5 layers (Fig.12a). Tamm plasmon state localizes at the edge between a thin metal layer and the distributed Bragg reflector (DBR) structure. The ultra-strong interaction and the exchange of energy between light and matter leads to formation of polaritons that were revealed as a splitting of polariton branches in optical spectra. Theoretically predicted possibility of the opposite sign of the polarization splitting for the lower and upper polariton branches (LP and UP) in the ultra-strongly coupled organic Tamm plasmon cavity was experimentally demonstrate at room temperature. Organic material was DPAVBi (4,4′-Bis[4-(di-p-tolylamino)styryl]biphenyl) (Fig.12b). The optical properties of the DPAVBi and the cavity are shown in Fig.12c. A high oscillator strength of exciton in DPAVBi provides interaction of Tamm plasmon and exciton in ultrastrong coupling regime when the values of the Rabi splitting is close to 20% fraction of the exciton energy. The model predicts the opposite sign of the polarization splitting for the low and upper polariton cases unlike splitting in semiconductor microcavities. Measured angle-dependent reflectivity spectra of the structures for both TE and TM polarizations (Fig.13a,b and c,d) confirmed the predicted theoretical assumption. We obtained a giant value of the polarization splitting up to 180 meV for both polariton branches as shown in Fig.14 for theory and experiment.

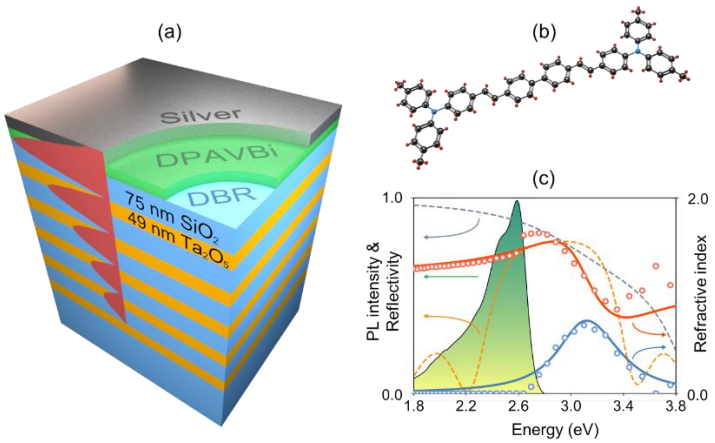

Figure 12. (a) Scheme of the Tamm plasmon cavity with SiO_2/ Ta_2O_5 DBR, DPAVBi layer ans 50 nm silver layer. The red area demonstrates the Tamm plasmon electric field profile (b) The scheme of the DPAVBi molecule structure. (c) Optical properties of the cavity and the molecule. Left axis: steady-state photoluminescence (PL) spectra of the bare DPAVBi molecule (green area), the reflectivity spectrum of the DBR structure (orange dashed curve) and the 50 nm silver later (grey dashed curve); Right axis: Real (red line and circles) and imaginary (blue line and circles) parts of the DPAVBi refractive index. The circles are the experimental data and the solid curves show the theoretical fit.

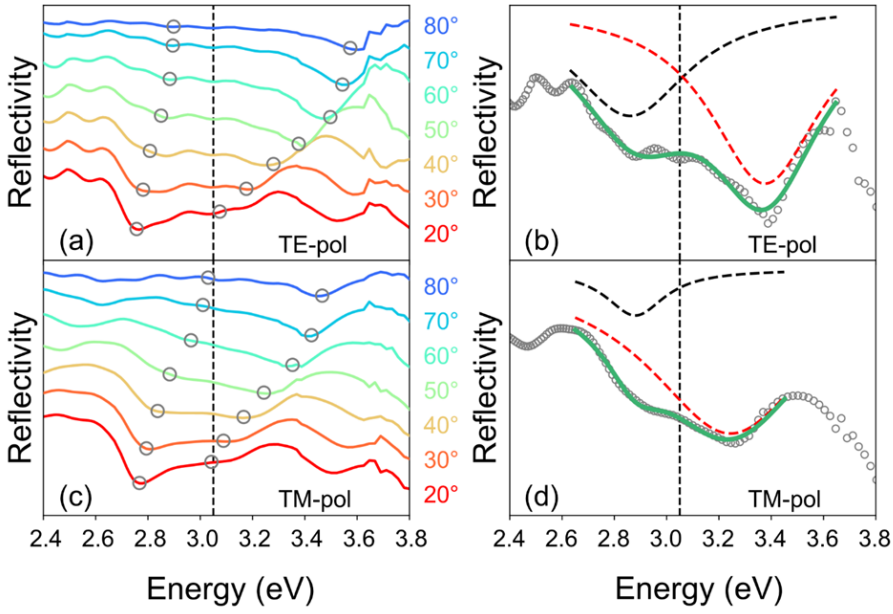

Figure 13. (a,c) Angle dependent reflectivity spectra of the sample with 21 nm DPAVBi/Tamm plasmon cavity measured in two polarization: TE and TM. Grey circles show the positions of the dips corresponding to the low (LP) and upper (UP) polaritonic states obtained by fitting. The right graphs (b,d) show examples of fitting of the reflectivity spectrum measured at 50 degree (grey circles) using Lorentz function. Black dashed lines demonstrate the fit of the LP-branch dip, red dashed lines show the UP-branch dip fit. The green curves show cumulative fit function. The vertical black dashed lines demonstrate the energy of the DPAVBi exciton.

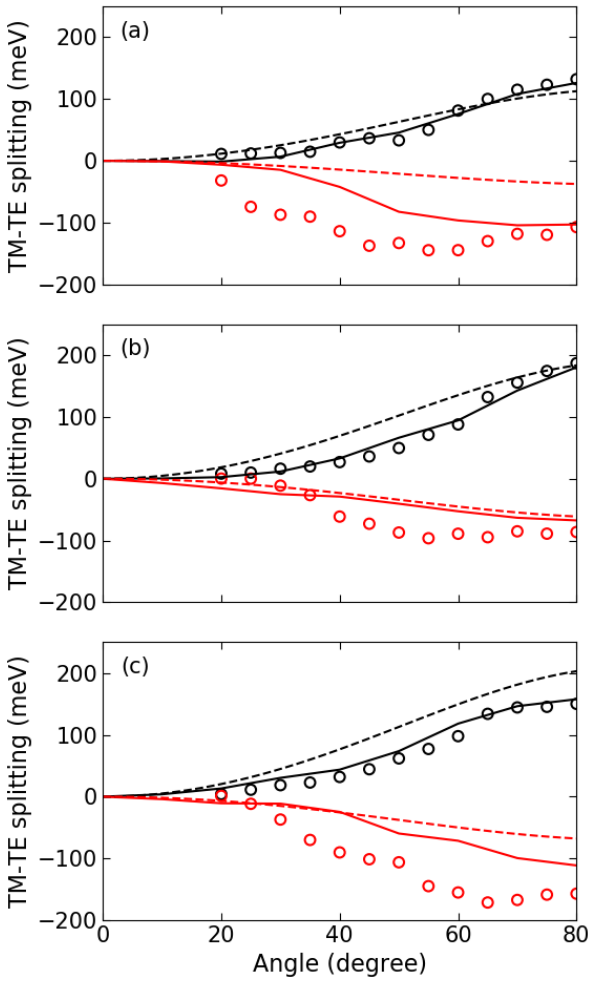

Figure 14. Angle dependence of the TM-TE polarization splitting of the LP (black curves and circles) and the UP (red curves and circles) states for the 21 nm (a) 40 nm (b) and 60 nm (c) structures. Circles are the fit of the experimental results, dashed curves – analytical model results, solid curves represent the results of the numerical reflectivity spectra fit.

We observed non-linear optical effects in planar GaN nanowires in the case when the nanostructure contains a structural defect such as stacking faults (SFs). Importantly, a single SF in this material plays the role of the quantum well, which allows the localization of excitons. The emission spectra in planar nanowires with SFs show clear SF-related optical signatures, while NWs without SFs demonstrate only excitonic-related transition (see Fig.15a and b, respectively). PL peaks with energy positions of ~3.48 eV, 3.43 eV and 3.34 eV at 5 K are denoted as X, SF1 and SF2, respectively. The most significant result is related to a super-linear (approximately quadratic) increase of integrated photoluminescence (PL) intensity with increasing excitation power for the exciton localized at SFs compared with bulk exciton as shown in Fig.16 a and b, respectively. The effect was explained by interaction of exciton with cavity modes. Theoretical calculations have shown that cavity modes with smaller volume (and, thus, with high values of Q-factor), which

can interact with exciton more efficiently, are localized at the edges of the structure (Fig.165c).

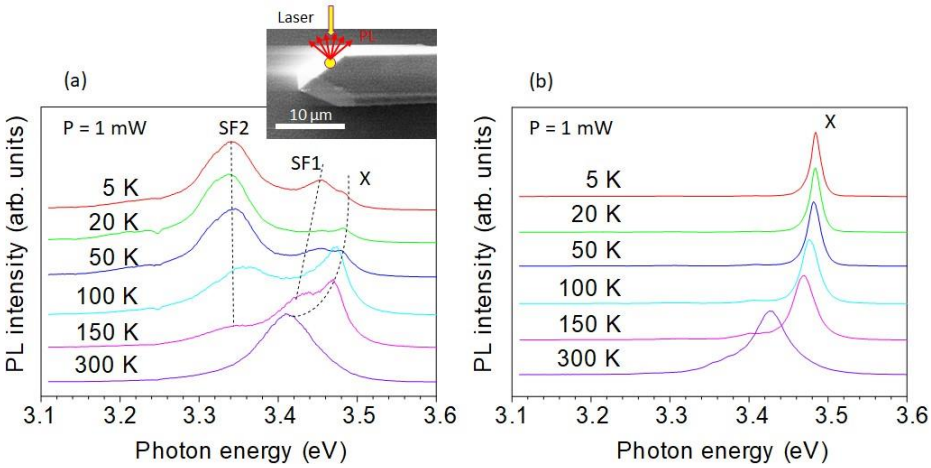

Figure 15. Temperature-dependent behavior of PL spectra measured for the planar GaN nanowire. (a) Spectra taken at nanowire with SF show besides exciton X also two emission bands SF1 and SF2 related to stacking faults. Dashed lines are guides for the eye. The inset shows schematically the incidence of the laser beam. (b) PL spectra taken at the nanowire with no SF show only excitonic-related emission X. PL spectra are normalized and vertically shifted for clarity.

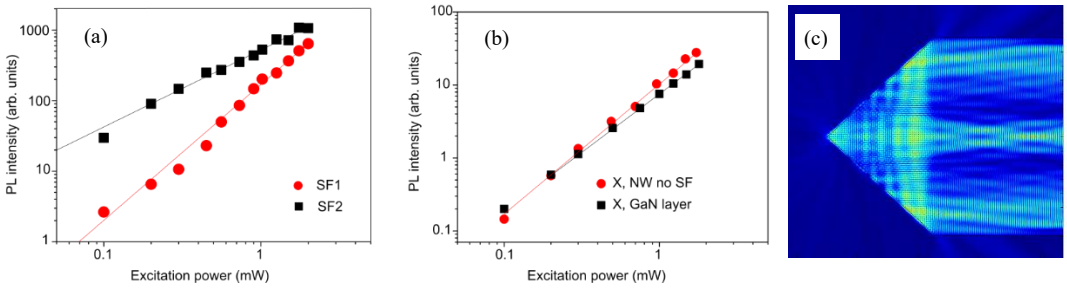

Figure 16. (a) Dependence of the integrated PL intensity for the SF1 and SF2 emissions (in Fig.15a) on the excitation power. (b) Integrated PL intensity for the X line vs excitation power for planar nanowire without SFs and for the GaN layer. (c). Distribution of the eigenmode field with an energy of 3.4601 eV and Q-factor 2.07×10^5 at the edge of the structure.

We have also developed a growth process to produce InGaN structures with different In fraction composition, since with increasing In the operation region can be shifted to green and yellow spectral range. A plasma-assisted halide phase vapor epitaxy (PA-HVPE) approach was demonstrated for the manufacture of In GaN layers at ~600 °C (see Methods). We solved the problem related to the activation of ammonia, which is a precursor for nitrogen in the epitaxial growth of III-nitrides. In order to grow InGaN with high In contents, the temperature must be drastically lowered (from 1000 °C) and this means that the ammonia is not decomposed effectively, which prevents growth and results in bad quality of material. Using plasma source introduced in the epitaxial reactor, we managed to activate ammonia and to synthesize InGaN heteroepitaxial layers. The incorporation of indium was confirmed by XRD, SIMS, and absorption measurements, but does not exceed 8%. The band gap shift to lower energies caused by different concentrations of indium in the InGaN layers was clearly observed in transmission measurements. The

optical band gap was estimated from the absorption coefficient α. For the direct band gap semiconductors α is related to the band gap energy E_g as follows:

$$\alpha^2 E^2 \sim (E - E_g),$$

where E is the photon energy. Graphs of α^2E^2 as a function of photon energy in the vicinity of the band edge are shown in Fig.17a for samples grown with different HCl flows through the boat with indium. The reference spectrum for the GaN template is also shown in the inset. The shift in the absorption edge was clearly seen in Fig.17b for the samples grown using different temperatures of the indium melt. The energy of the band gap was estimated by extrapolating the linear part of α^2E^2 to zero as indicated by dashed lines. The extracted values of E_g are plotted in Fig. 18. Note, the optical band energy of 3.396 eV estimated for the GaN template is slightly higher than the 3.39 eV for relaxed GaN, which is common for layers under compression when grown on sapphire.

We found tha although plasma is very efficient to activate ammonia and to increase the growth rates at low temperatures, the concentration of indium significantly reduces due to the activation of reactive chlorine-containing species that etch In at the growth surface. To increase the efficiency of the indium precursor, further modifications of the gas inlets and the plasma source should be done. To avoid the negative effect of chlorine species on the structural quality and the in-corporation of indium into InGaN layers, the supply of GaCl and InCl/InCl3 precursors should approach the growth surface without passing through the plasma source. Nevertheless, the suggested PA-HVPE process is very promising for activating ammonia and promoting the growth of thick III-nitrides layers at low temperatures. However, the In concentration was low, in the order of a few percent, as the incorporation of In is reduced by plasma due to the activation of chlorine-containing species that etch the relatively poorly bonded In atoms. Nevertheless, the approach of using plasma for ammonia activation is a very promising approach to growing epitaxial III-nitrides at low temperatures.

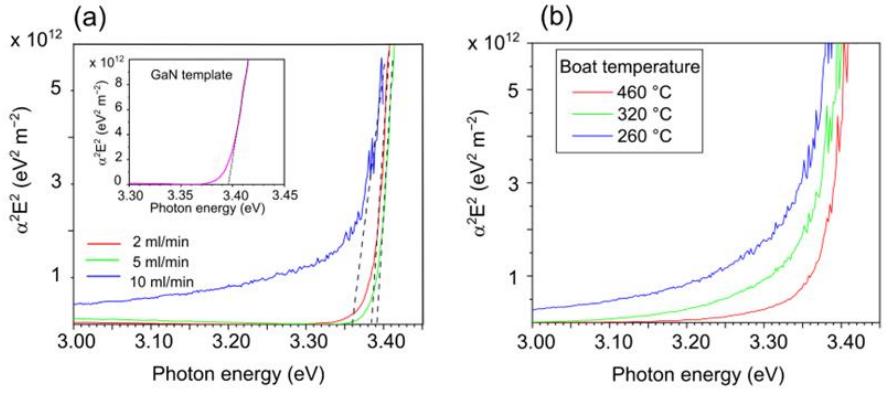

Figure 17. (a) Squared absorption coefficient plotted as a function of photon energy for layers grown at 570 °C at three different flows of HCl through the boat with indium. Temperature of the boat kept constant at 320 °C. The inset shows the spectrum for the GaN template for reference. The dashed lines are a guide to the eye. (b) Graphs for layers grown at 620 °C for different temperatures of the boat with metallic indium. HCl flow over indium melt was kept to 5 mL/min.

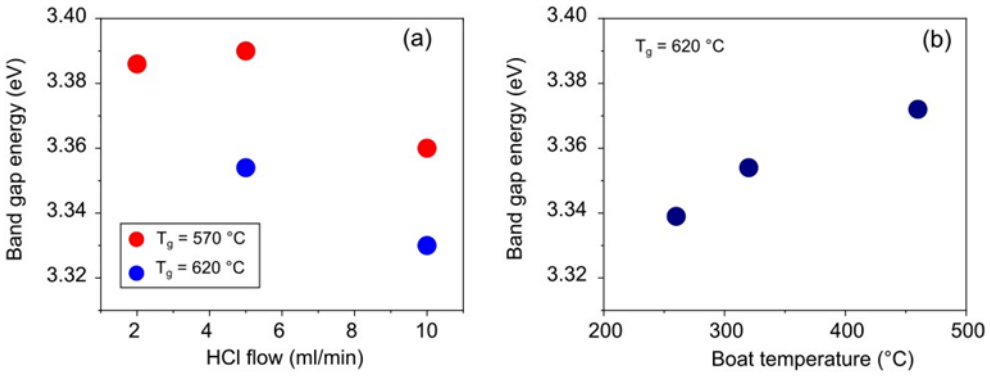

Figure 18. The band gap energy estimated from the absorption measurements for samples grown (a) with different HCl flows through the boat with indium and (b) at different temperatures of the boat with indium.

The combination of unique properties exhibited by semiconductor nanowires (NWs) and the interesting properties of metal nanoparticles (NPs) enables the creation of hybrid nanostructures with a high degree of design freedom. Plasmonic nanoparticles (NPs) that can interact with light and can significantly enhance the excitation of semiconductors due to the localized plasmon resonance [4]. In addition, plasmonic properties can vary depending on the size and shape of NPs and the metal used [5]. Silver NPs have a resonance frequency from the near-UV to visible regions depending on the NP size (see Fig.19a) and for small Ag NPs, there is a good overlapping between their absorption and GaN emission spectra. We have studied plasmonic properties of hybrid nanoantenna structures formed by Ag NPs with a radius of 30 nm (Fig.19b) and GaN planar nanowires grown along [10-10] in-plane crystallographic directions. Silver NPs of a spherical shape with a radius of 30 nm have a localized plasmon resonance around 400 nm. We found in hybrid structures (see Fig. 20a) an appearance of new narrow emission line at ~3.36 eV as shown in Fig.20b.

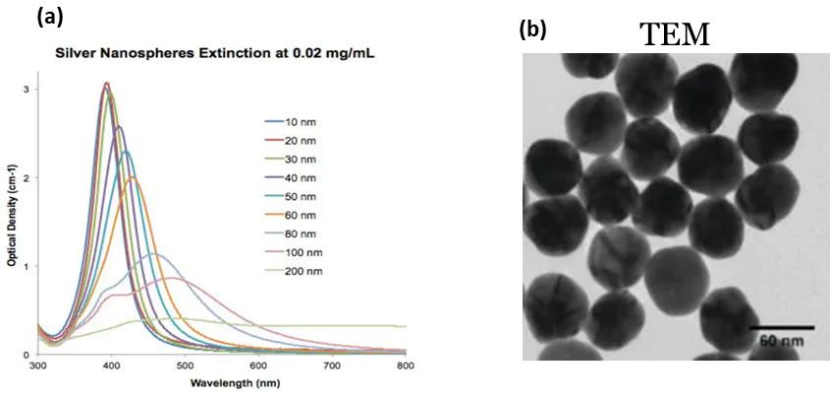

Figure 19. (a) Optical density spectra for spherical Ag NPs with different size. (b) TEM image of Ag NPs with a size of 60 nm.

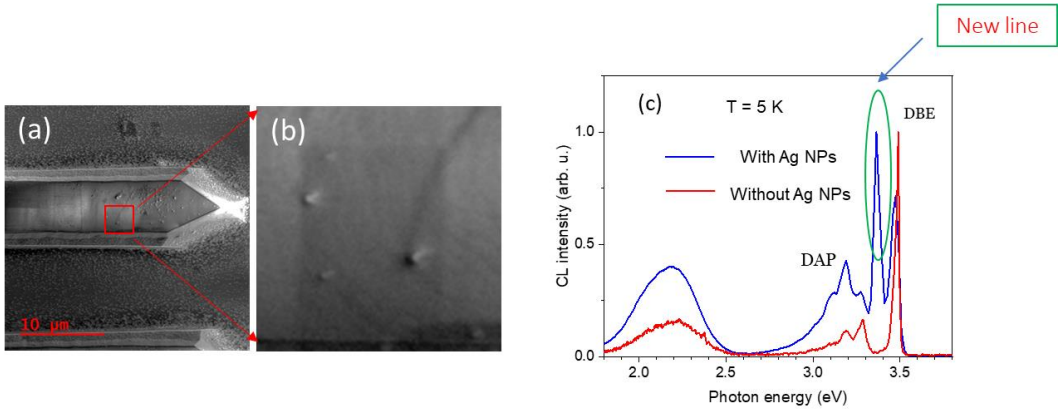

Figure 20. (a) Overview of SEM image of the planar GaN NW without Ag NPs. (b) Enlarged SEM image showing Ag NPs on the surface. (c) Normalized cathodoluminescence (CL) spectra taken at 5 K for GaN NW without Ag NPs (red line) and with Ag NPs (blue line).

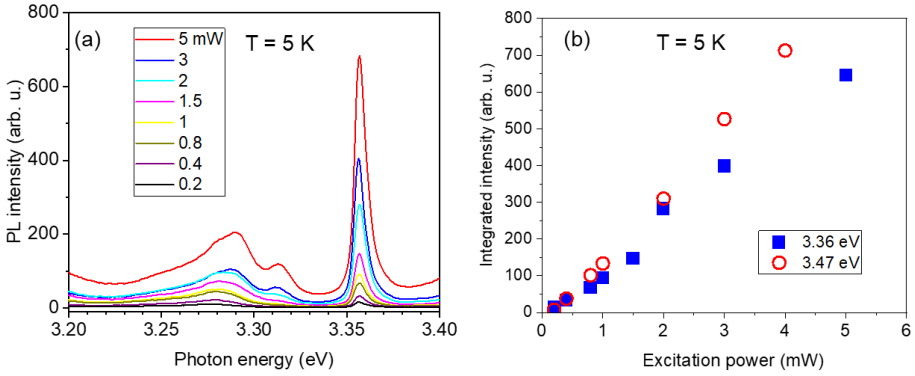

Figure 21. (a) Photoluminescence (PL) spectra taken at 5 K at different excitation powers for the hybrid Ag NPs/GaN NW structure. Spectra are shown in the region around the 3.36 eV line. (b) Integrated PL intensity measured at 5 K for the 3.36 eV line (closed squares) and for the 3.47 eV DBE emission (open circles) vs excitation power.

We studied both temperature and power dependence of the new line in emission spectra. The line is thermolyzed at 50 K and the power dependence is linear, which indicates that the new line is not related to cavity mode or lasing.

To explain the enhancement of emission lines in the luminescence spectra of the hybrid Ag NPs/GaN NWs structure, we considered a theoretical model based on Fröhlich approximation. The electric field of the light induces polarization, and a small particle can be considered a radiative dipole. In this case, a resonant feature in the spectra of spherical metal nanoparticles is expected to occur near the wavelength that satisfies the Fröhlich condition:

$$Re\{\varepsilon(\omega)\} = -2Re\{\varepsilon_m(\omega)\}$$

where ε and ε_m are the dielectric constant of the metal and the medium, respectively. In the general case, the scattering of spherical particles is described

using the Mie theory, which gives the scattering and extinction cross-sections as a sum of the electric and magnetic spherical waves (harmonics). Dipole scattering describing the Fröhlich resonance is given by the electric harmonic with the quantum number $l = 1$ [6,7].

The scattering cross-section spectrum (that correlate with luminescence) was calculated for a bare Ag NP in air, resulting in the peak position of the resonance of 3.42 eV, i.e. at lower energy compared to the observed experimental line. To obtain a correlation with the experiment, we also considered an oxidized Ag NP and the effective medium approach. The latter approach was adopted because the Ag NP had a non-zero contact area with the GaN NW surface. The presence of the GaN substrate shifted the position of the resonance to the low-energy region, and the effective medium consisting of air and 10% GaN described the experimental results well. The model with effective medium approximation is the most realistic one.

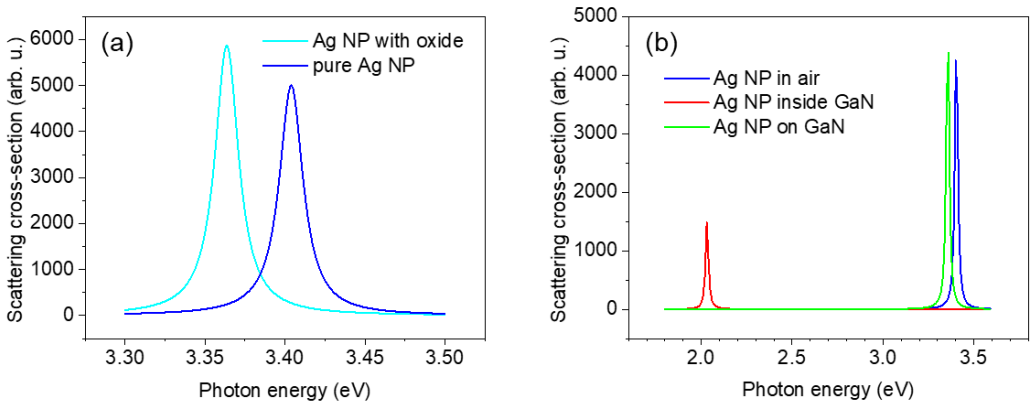

Figure 22. (a) The scattering cross-section spectra calculated for a bare silver nanoparticle in air (blue line) and for the Ag NP covered with a 1.5 nm thin oxide film (cyan line). (b) The scattering cross-section spectra are compared for the Ag NP in air (blue line), embedded in GaN (red line), and placed on the GaN surface with contact area of 10 % (green line).

How the Ag NPs can modify emission properties of semiconductor nanostructures has been studied further using similar GaN planar NWs grown, however, along the [11-20] in-plane crystallographic direction. In this case, the GaN NWs exhibit a number of structural defects, such as stacking faults (see Fig. B1 in bilaga "Känslig information"). The hybrid structure was formed by Ag NPs with a 60 nm diameter and GaN NWs (example is shown in Fig. B2 in bilaga "Känslig information"). Stacking faults in the bare GaN NWs have well-known optical signatures with the emission bands at ~3.44 eV and ~3.33 eV (SF1 and SF2 in Fig. B3a in bilaga "Känslig information"). Hybrid structure demonstrates a modified PL spectrum where two distinct and narrow lines appear at ~3.36 eV and 3.31 eV, labelled as FR1 and FR2, respectively, with relative intensities varied within the nanostructure (Fig.B3b in bilaga "Känslig information").
In this case, simple Fröhlich approximation does not explain appearance of two new lines in the hybrid nanostructure. Our theoretical model relies on the method of images of charges, accounting for the influence of the substrate on the polarizability

tensor (see Fig.B4 in bilaga “Känslig information”). It considers both the quadrupole moment of the sphere and the quadrupole field of the image, providing a comprehensive explanation for the observed experimental results (see text and Fig.B5 in bilaga “Känslig information”). The obtained two resonance peaks in the calculated scattering cross-section spectra for a silver nanoparticle placed on a GaN substrate have frequencies of 3.31 eV and 3.36 eV, which are in very good agreement with the experimental features in the PL spectrum.

While structures for nanoantenna are under intensive development and studies, the problems remain regarding the design of rectifying diodes that can respond effectively to optical frequencies, which corresponds to wavelengths in the visible, infrared, and ultraviolet regions, and, thus, are extremely high. Despite promising efforts for tunneling diodes in the terahertz region [8], these electronic elements remain the main challenge in realization of optical rectenna. We, therefore, have studied the possibility of growing wide bandgap semiconductors on the device structures that need an efficient and stable absorber of solar energy in water splitting systems, which is a promising method for H_2 production We have used HVPE process for synthesis of Ga metal compounds materials, especially, gallium oxide, for this purpose and preliminary, we have observed a very promising contribution of our materials to stability and enhanced performance of the photocathode devices for photoelectrochemical water splitting, making them valuable components for sustainable energy applications (see Figure B7 and description in bilaga “Känslig information”).

Diskussion

The results of the study reveal a significant effect of the crystallographic growth direction on the structural quality of planar GaN nanostructures, particularly along [11-20] and [10-10] directions. This finding suggests that these nanowires can be effectively utilized as optical resonators and building blocks for nano-antennas in the development of advanced optoelectronic devices. The presence of Fabry-Perot modes further confirms the high quality and resonator properties of the nanostructures along the [10-10] direction. Furthermore, we have explored other types of GaN planar nanostructures, such as hexagons, which exhibit modifications in emission spectra due to interactions between excitons and cavity modes. The understanding of the emission characteristics in different nanostructures is important for the design of energy-efficient devices. The ability to control the crystallographic growth direction and optimize the properties of GaN nanostructures opens avenues for enhancing the efficiency of optoelectronic devices and to improved performance in light absorption and emission processes, that can be utilized for increasing efficiency and performance of solar energy harvesting and conversion.

Our studies on plasmonic-polaritonic phenomena in layered structures provides insights into reducing losses, offering design principles for enhancing spontaneous

emission probabilities in visible or infrared energy regions. The observed non-monotonic emission behavior in planar nanocavities under optical pumping suggests potential for novel non-linear applications. Exploring the interaction of light and matter in strong and ultra-strong coupling regimes, particularly in Tamm plasmon cavities at room temperature creates several potential roots for advancements in technologies relying on light-matter interactions that could lead to more efficient PV and optoelectronic devices. Observed non-linear effects in GaN nanostructures opens opportunities for improving light emission properties through understanding the interaction of excitons with cavity modes in meso-cavities that much easily can be produced compared with vertical microcavities that need complicated distributed Bragg reflectors.

The development of a plasma-assisted halide phase vapor epitaxy (PA-HVPE) process for growing InGaN layers at lower temperatures. This process provides control over the indium fraction composition, facilitating shifts in the operation region towards the green and yellow spectral ranges. This can be important in addressing the challenges of developing rectifying diodes operating at ultra-high frequencies. However, challenges, such as the reduction of indium concentration due to plasma activation, indicate the need for further modifications in the growth process. Future research should focus on optimizing the gas inlets and plasma source to enhance the efficiency of the indium precursor while maintaining structural quality. To avoid the negative effect of chlorine species on the structural quality and the in-corporation of indium into InGaN layers, the supply of GaCl and $InCl/InCl_3$ precursors should approach the growth surface without passing through the plasma source. Despite challenges, the suggested PA-HVPE process shows promise for activating ammonia and promoting the growth of thick III-nitride layers at low temperatures, which is also contribution to energy-efficient semiconductor manufacturing processes. Moreover, the potential of wide bandgap semiconductors, especially gallium oxide, was explored for producing device structures with applications in photoelectrochemical water splitting. Preliminary observations suggest promising contributions to the stability and performance of photocathode devices, in line with sustainable energy applications.

The combination of semiconductor nanowires (NWs) and metal nanoparticles (NPs) in hybrid nanostructures provides a platform with diverse design possibilities. Plasmonic nanoparticles, particularly silver NPs, can interact with light and enhance semiconductor excitation through localized plasmon resonance. This interaction, dependent on NP size and shape, offers a spectrum of interesting properties improving performance of various applications such as in photovoltaics, biosensing, and LEDs. For instance, silver NPs with a radius of 30 nm exhibit a resonance frequency spanning from near-UV to visible regions, aligning well with the emission spectra of GaN. Our study have revealed that hybrid nanostructures demonstrate a modified optical property compared to bare GaN nanostructures with the appearance of new emission lines. To explain the new emissions in hybrid structures, a theoretical model based on Fröhlich approximation was employed. The model considers the electric field-induced polarization, treating the metal NP as a radiative dipole. The presence of semiconductors (GaN structures) together with the size of metal particle has a crucial role on the frequency of the modified spectra.

Theoretical models based on the method of images of charges, accounting for substrate influence, provide a more comprehensive explanation for these observations. This insight contributes to the understanding of emission properties in hybrid nanostructures and is a key to design nanoantenna that can be used for harvesting electromagnetic radiation with different frequency. Significant challenges in nanoantenna design, however, are related to rectifying diodes that still need to be developed for effective operation at optical frequencies, particularly in the infrared and visible regions.

The research provided valuable insights into control and manipulating emission properties of materials for sustainable energy applications. Continued investigation is imperative to overcome challenges in design and optimization of growth methods, including the possibility of control electrical doping without degrading material quality.

The obtained results contribute to the development of energy-efficient technologies and sustainable energy systems, improving efficiency and providing new methods for growing III-nitride semiconductors of electronic quality at lower temperatures. The project results play an important role in enhancing our understanding of nanomaterials and the influence of metal nanostructures on optical properties, paving the way for the development of devices that can harness solar energy more effectively. This advancement, in turn, contributes to the transition towards clean and renewable energy sources, addressing environmental concerns associated with traditional energy production methods.

Publikationslista

1. G. Pozina, K.A. Ivanov, M.I. Mitrofanov, M.A. Kaliteevski, K.M. Morozov, I.V. Levitskii, G.V. Voznyuk, V.P. Evtikhiev, S.N. Rodin. Optical cavity based on GaN planar nanowires grown by selective area metal-organic vapor phase epitaxy. *Phys. Status Solidi B* **256** (6), 1800631 (2019).

The paper studies GaN planar nanowires (NWs) fabricated using pattering with focused ion beam etching. The NWs grown along [10-10] direction exhibit superior morphology, crystalline, and optical properties, including Fabry-Perot modes revealed by cathodoluminescence.

2. A.V. Belonovskii, I.V. Levitskii, M.I. Mitrofanov, E.I. Girshova, K.A. Ivanov, S.N. Rodin, K.M. Morozov, V.P. Evtikhiev, M.A. Kaliteevski. Emission properties of GaN planar hexagonal microcavities. G. Pozina, C. Hemmingsson, *Phys. Status Solidi A* **217**, 1900894 (2020).

In this paper, we propose a planar GaN microresonator design as hexagonal microstructures. Cathodoluminescence reveals dominant emission lines in the near band gap region different compared with excitonic emission and merging at room

temperature into a broad band peaking at ~3.3 eV. Numerical analysis indicates that strongly localized cavity modes with high Purcell coefficients can interact with GaN excitons and enhance emission.

3. A.V. Belonovski, I.V. Levitskii, K.M. Morozov, G. Pozina, M.A. Kaliteevski. Weak and strong coupling of photons and excitons in planar meso-cavities. *Optics Express* **28** (9), 12688-12698 (2020).

We have studied exciton-cavity mode interactions in planar meso-cavities with sizes a few wavelengths, when the frequency interval between optical modes is comparable to or smaller than the Rabi splitting. The Hamiltonian is constructed, showing this interaction in weak and strong coupling regimes. Strong coupling results in pronounced emission peak splitting in modeled meso-cavities, revealing significant differences in Q-factors and interaction strengths among adjacent cavity modes.

4. K.A. Ivanov, K.M. Morozov, G. Pozina, A.R. Gubaydullin, E.I. Girshova, M.A. Kaliteevski. Control of the surface plasmon dispersion and Purcell effect at the metamaterial-dielectric interface. *Scientific Reports* **10**, 20828 (2020).

We investigated the use of metamaterials to mitigate absorption effects in metals on the Purcell factor. The study explored surface plasmon dispersion and peak position in the local density of states for different material combinations and filling factors. Calculated Purcell factor frequency dependence has shown an increased peak value compared to conventional plasmonic structures.

5. G. Pozina, C.W. Hsu, N. Abrikossova, M.A. Kaliteevski, C. Hemmingsson. Development of β-Ga_2O_3 layers growth on sapphire substrates employing modeling of precursors ratio in halide vapor phase epitaxy reactor. *Scientific Reports* **10**, 222061 (2020).

We have developed a halide vapor phase epitaxy reactor and optimized the growth process for wide bandgap semiconductor Ga_2O_3. The structural and optical quality was studied depending on temperature and substrate orientation.

6. A.V. Belonovski, K.M. Morozov, E.I. Girshova, G. Pozina, M.A. Kaliteevski. Quantum analysis of luminescence of an exciton in a meso-cavity. *Optics Express* **29** (13), 20724-20734 (2021).

Interaction of cavity modes with exciton in meso-cavity has been analyzed using a quantum-mechanical approach. Simultaneous interaction of exciton and several cavity modes results in novel effects such as quantum beating and non-monotonic dependence of ground polariton state in the system on the pumping.

7. G. Pozina, C.-W. Hsu, N. Abrikossova, C. Hemmingsson. Doping of β-Ga_2O_3 layers by Zn using halide vapor-phase epitaxy process. *Phys. Status Solidi* A **218**, 2100486 (2021).

We investigated the possibility to use metal pallets for in situ producing precursors for electrical doping use halide vapor phase epitaxy. A good Zn doping concentrations was achieved. We found that Zn doping does not affect optical properties, but oxygen-rich conditions and crystalline particle formation modify the luminescence spectra.

8. K.M. Morozov, P. Pander, L.G. Franca, A.V. Belonovski, E.I. Girshova, K.A. Ivanov, D.A. Livshits, N.V. Selenin, G. Pozina, A.P. Monkman, M.A. Kaliteevski. Opposite sign of polarization splitting in ultrastrongly coupled organic Tamm plasmon structures. *J. Phys. Chem. C* **125** (15), 8376-8381 (2021).

We investigated the ultrastrongly-coupled Tamm plasmon cavity filled with the high oscillator-strength organic material DPAVBi. Theoretical methods predicted a giant polarization splitting with an opposite sign for LP and UP cases. Experimental results confirmed the predicted polarization splitting behavior, reaching up to 180 meV for both polariton branches—a unique demonstration in the ultrastrong coupling regime.

9. E.I. Girshova, G. Pozina, A.V. Belonovskii, M.I. Mitrofanov, I.V. Levitskii, G.V. Voznyuk, V.P. Evtikhiev, S.N. Rodin, M.A. Kaliteevski. Enhancement of the basal-plane stacking fault emission in GaN planar nanowire microcavity. *JETF Letters* **115** (10), 574-580 (2022).

We have compared optical microcavities formed by GaN planar nanowires, considering structures with and without stacking faults. The study explores non-linear behavior of an exciton localized in a stacking fault, revealing distinct variations in photoluminescence intensity and decay time. Theoretical calculations indicate field localization at the ends of the structure.

10. G. Pozina, C.-W. Hsu, N. Abrikossova, C. Hemmingsson. Numerical modelling for the experimental improvement of growth uniformity in a halide vapor phase epitaxy reactor for manufacturing β-Ga_2O_3 layers. *Crystals* **12**, 1790 (2022).

We have optimized the halide vapor phase epitaxy (HVPE) process for growing gallium oxide layers and improved growth uniformity. Numerical calculations have been performed to calculate the distribution of gas flows over sample holder using different design of the gas inlet. The optimized geometry was confirmed by experimental results.

11 G. Pozina, C.-W. Hsu, N. Abrikossova, Carl Hemmingsson. Plasma-assisted halide vapor phase epitaxy for low temperature growth of III-nitrides. *Crystals* **13**, 373 (2023).

We have developed plasma-assisted halide phase vapor epitaxy for low-temperature growth of III-nitride semiconductors, which is crucial for enhancing activation of ammonia at ~600 °C, and thus, increasing the growth rate from ~1.2 to ~4–5 µm/h. We have demonstrated the growth of InGaN at ~600 °C, achieving moderate In concentration of several %, which was caused by to the plasma activation of chlorine-containing species.

12. G. Pozina, C. Hemmingsson, N. Abrikossova, E.I. Girshova, E. Lahderanta, M.A. Kaliteevski. Effect of plasmonic Ag nanoparticles on emission properties of planar GaN nanowires. *Nanomaterials* **13** (8), 1421 (2023).

We have prepared hybrid nanostructures combining plasmonic Ag nanoparticles with planar GaN nanowires (NWs). We have observed a strong modification in emission spectra of hybrids compared to bare NWs. A new emission line at 3.36 eV appears when measured near the Ag NPs. A model based on the Fröhlich resonance approximation explains the results, with the effective medium approach describing the enhanced emission features near the GaN band gap.

Referenser, källor

[1]. Bean, J. A.; Weeks, A. & Boreman, G. D. Performance optimization of antenna-coupled Al/AlOx /Pt tunnel diode infrared detectors. *IEEE J. Quantum Electron*. **47**, 126–135 (2011).

[2]. Yam, F.K.; Hassan, Z. InGaN: An overview of the growth kinetics, physical properties and emission mechanisms. *Superlattices and Microstructures* **43**, 1–23 (2008).

[3]. Gérard, J.M.; Sermage, B.; Gayral, B.; Legrand, B.; Costard, E.; Thierry-Mieg, V. Enhanced Spontaneous Emission by quantum boxes in a monolithic optical microcavity. *Phys. Rev. Lett*. **81**, 1110 (1998).

[4]. Fadil, A.; Ou, Y.; Iida, D.; Kamiyama, S.; Petersen, P.M.; Ou, H. Combining surface plasmonic and light extraction enhancement on InGaN quantum-well light-emitters. *Nanoscale* **8**, 16340–16348 (2016).

[5]. Pescaglini, A.; Iacopino, D. Metal nanoparticle–semiconductor nanowire hybrid nanostructures for plasmon-enhanced optoelectronics and sensing. *J. Mater. Chem. C* **3**, 11785–11800 (2015).

[6]. Fan, X.; Zheng, W.; Singh, D. Light scattering and surface plasmons on small spherical particles. *Light Sci. Appl*. **3**, e179 (2014).

[7]. Luk'yanchuk, B.S.; Tribelsky, M.I.; Ternovsky, V.; Wang, Z.B.; Hong, M.H.; Shi, L.P.; Chong, T.C. Peculiarities of light scattering by nanoparticles and

nanowires near plasmon resonance frequencies in weakly dissipating materials. *J. Opt. A Pure Appl. Opt.* **9**, S294–S300 (2007).

[8]. Belkadi, A.; Weerakkody, A.; Moddel, G. Demonstration of resonant tunneling effects in metal-double-insulator-metal (MI2M) diodes. *Nature Commun*. **12**, 2925 (2021).

Bilagor

1 KÄNSLIG INFORMATION.

Bilaga “KÄNSLIG INFORMATION” should not be published in the database since the results are subject to articles currently under preparation, and therefore, the results and figures cannot be made public.